INTERNATIONAL JOURNAL FOR NUMERICAL METHODS IN FLUIDS
Int. J. Numer. Meth. Fluids 2000; **32**: 349–364

Colocated schemes for the incompressible Navier–Stokes equations on non-smooth grids for two-dimensional problems

C. Moulinec and P. Wesseling*

Faculty of Information Technology and Systems, Delft University of Technology, Mekelweg 4, 2628 CD Delft, Netherlands

SUMMARY

The accuracy of colocated finite volume schemes for the incompressible Navier–Stokes equations on non-smooth curvilinear grids is investigated. A frequently used scheme is found to be quite inaccurate on non-smooth grids. In an attempt to improve the accuracy on such grids, three other schemes are described and tested. Two of these are found to give satisfactory results. Copyright © 2000 John Wiley & Sons, Ltd.

KEY WORDS: colocated schemes; incompressible Navier–Stokes; finite volume methods

1. INTRODUCTION

For the numerical solution of the incompressible Navier–Stokes equations on a structured boundary-fitted grid, a colocated grid is more widely used than a staggered grid. The reason is that accurate discretization on curvilinear grids is more straightforward. The accuracy depends on the way in which derivatives are approximated at cell faces. In earlier publications, e.g. [1–3], this has been accomplished by what is called the two-point method or the TP method for short. It will be shown that this gives inaccurate results on non-smooth curvilinear grids. Since, in practical engineering computations, the use of locally strongly distorted and non-uniform grids is frequently unavoidable, discretizations that maintain accuracy under these circumstances are useful. Three alternatives for improvement will be investigated. The first method (called the BI method for short) used bilinear interpolation. The second (called the PI method) uses the path–integral method described in [4–6]. The third (called the AUX method) uses auxiliary points, and is a generalization of a method proposed in [7].

* Correspondence to: Faculty of Information Technology and Systems, Delft University of Technology, Mekelweg 4, 2628 CD Delft, Netherlands.

CCC 0271–2091/2000/030349–16$17.50

Received 20 October 1998
Revised 9 February 1999

2. DISCRETIZATION IN CURVILINEAR CO-ORDINATES

2.1. Transformation to curvilinear co-ordinates

It is sufficient to consider the two-dimensional case. A boundary-fitted co-ordinate transformation $\boldsymbol{x} = \boldsymbol{x}(\boldsymbol{\xi})$ is assumed, mapping a rectangle G in the computational $\boldsymbol{\xi}$ plane onto the flow domain in the physical $\boldsymbol{x}$ plane, which results in the following identity [8]:

$$\frac{\partial}{\partial \xi^\alpha}(\sqrt{g}\boldsymbol{a}^{(\alpha)}) \equiv 0, \tag{1}$$

where $\sqrt{g}$ is the Jacobian of the mapping $\boldsymbol{x} = \boldsymbol{x}(\boldsymbol{\xi})$ and $\boldsymbol{a}^{(\alpha)} = \nabla \xi^\alpha$. The summation convention is used throughout. This allows the chain rule to be written as follows:

$$\frac{\partial \phi}{\partial x^\alpha} = \frac{1}{\sqrt{g}} \frac{\partial}{\partial \xi^\beta}(\sqrt{g} a_\alpha^{(\beta)} \phi). \tag{2}$$

The governing equations are transformed from $\boldsymbol{x}$ into $\boldsymbol{\xi}$ co-ordinates. The dependent variables are not transformed. The momentum equations can be written as

$$\begin{aligned} &\frac{\partial \rho u^\gamma}{\partial t} + \frac{1}{\sqrt{g}} \frac{\partial \rho V^\alpha u^\gamma}{\partial \xi^\alpha} + \frac{\partial p}{\partial x^\gamma} - \frac{1}{\sqrt{g}} \frac{\partial \sqrt{g} a_\beta^{(\alpha)} \tau_\gamma^\beta}{\partial \xi^\alpha} = \rho f^\gamma, \\ &\tau_\gamma^\beta \equiv \mu \left(\frac{\partial u^\beta}{\partial x^\gamma} + \frac{\partial u^\gamma}{\partial x^\beta} \right), \\ &V^\alpha \equiv \boldsymbol{a}^{(\alpha)} \cdot \boldsymbol{u}, \end{aligned} \tag{3}$$

where u^γ is the Cartesian x^γ component of $\boldsymbol{u}$. Note that here the pressure gradient and the shear stress are not transformed. Discretization with the PI and AUX methods starts from Equation (3).

For the other two schemes, all terms are transformed to $\boldsymbol{\xi}$ co-ordinates, and (3) is rewritten as follows:

$$\frac{\partial \rho u^\gamma}{\partial t} + \frac{1}{\sqrt{g}} \frac{\partial \sqrt{g} a_\beta^{(\alpha)} \rho u^\beta u^\gamma}{\partial \xi^\alpha} + \frac{1}{\sqrt{g}} \frac{\partial \sqrt{g} a_\gamma^{(\alpha)} p}{\partial \xi^\alpha} - \frac{1}{\sqrt{g}} \frac{\partial}{\partial \xi^\alpha} \left(\sqrt{g} g^{\alpha\beta} \mu \left(\frac{\partial u^\gamma}{\partial \xi^\beta} + \frac{\partial u^\beta}{\partial \xi^\gamma} \right) \right) = \rho f^\gamma, \tag{4}$$

where $g^{\alpha\beta} \equiv \boldsymbol{a}^{(\alpha)} \cdot \boldsymbol{a}^{(\beta)}$.

2.2. Finite volume discretization

A uniform grid is given in G. The mapping $\boldsymbol{x} = \boldsymbol{x}(\boldsymbol{\xi})$ is assumed to be given in the nodes of G, and extended to all of G by piecewise bilinear interpolation; for details see [6]. This makes the mapping $\boldsymbol{x} = \boldsymbol{x}(\boldsymbol{\xi})$ piecewise differentiable, so that strongly non-uniform grids are allowed. The nodes are vertices of cells, which are unit squares in G, i.e. the mesh size satisfies $\Delta \xi^\alpha = 1$. The cells in Ω are quadrilaterals with straight edges.

The governing equations are integrated over a generic cell, Ω_h, in the physical domain. For the time derivative and the source term, this gives

$$\int_{\Omega_h} \frac{\partial \rho u^\gamma}{\partial t} \, \mathrm{d}\Omega \approx \sqrt{g}_{(0,0)} \frac{\mathrm{d}}{\mathrm{d}t} (\rho u^\gamma)_{(0,0)}, \qquad \int_{\Omega_h} \rho f^\gamma \, \mathrm{d}\Omega \approx \sqrt{g}_{(0,0)} (\rho f^\gamma)_{(0,0)}. \tag{5}$$

Positions in the grid in the vicinity of the generic cell Ω_h are denoted by subscripts (0, 0), etc., as indicated in Figures 1 and 2.

Derivatives with respect to ξ^α in (3) and in (4) are handled as follows. The viscous term in (3) and the inertia and pressure and terms in (4) can be subsumed under the following expression:

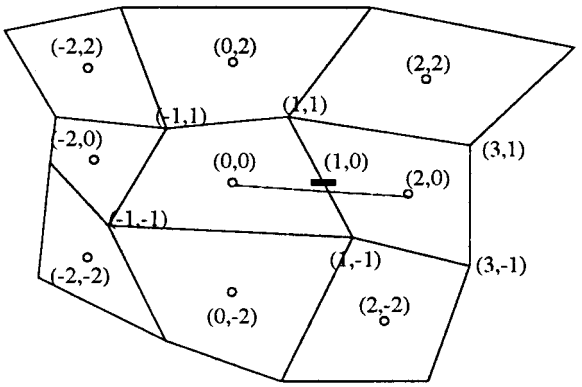

Figure 1. Example of physical domain.

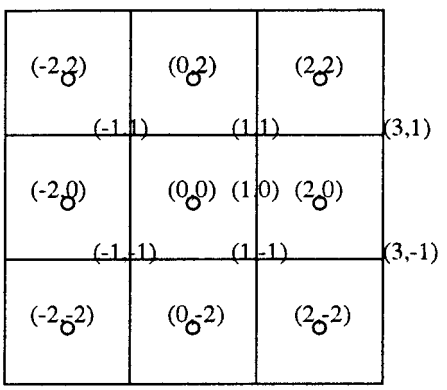

Figure 2. Computational domain.

$$\frac{1}{\sqrt{g}}\frac{\partial}{\partial \xi^{\alpha}}(\sqrt{g}a_{\delta}^{(\alpha)}\phi),$$

where $\delta=\beta$, $\phi=\tau_{\gamma}^{\beta}$ for the stress term; $\delta=\beta$, $\phi=\rho u^{\beta}u^{\gamma}$ for the inertia term; and $\delta=\gamma$, $\phi=p$ for the pressure term. Integration over Ω_h gives

$$\int_{\Omega_h}\frac{\partial\phi}{\partial x^{\delta}}\,\mathrm{d}\Omega=\int_{G_h}\frac{1}{\sqrt{g}}\frac{\partial}{\partial\xi^{\alpha}}(\sqrt{g}a_{\delta}^{(\alpha)}\phi)\sqrt{g}\,\mathrm{d}\xi^{1}\,\mathrm{d}\xi^{2}=\int_{G_h}\frac{\partial}{\partial\xi^{\alpha}}(\sqrt{g}a_{\delta}^{(\alpha)}\phi)\,\mathrm{d}\xi^{1}\,\mathrm{d}\xi^{2}$$
$$=(\sqrt{g}a_{\delta}^{(1)}\phi)|_{(-1,0)}^{(1,0)}+(\sqrt{g}a_{\delta}^{(2)}\phi)|_{(0,-1)}^{(0,1)}. \tag{6}$$

Similarly, for the integral of the viscous term in (4) over G_h, an expression of the following form results:

$$\int_{G_h}\frac{1}{\sqrt{g}}\frac{\partial}{\partial\xi^{\alpha}}\left(\sqrt{g}g^{\alpha\beta}\mu\frac{\partial u^{\varepsilon}}{\partial\xi^{\delta}}\right)\sqrt{g}\,\mathrm{d}\xi^{1}\,\mathrm{d}\xi^{2}=\left(\sqrt{g}g^{1\beta}\mu\frac{\partial u^{\varepsilon}}{\partial\xi^{\delta}}\right)\Bigg|_{(-1,0)}^{(1,0)}+\left(\sqrt{g}g^{2\beta}\mu\frac{\partial u^{\varepsilon}}{\partial\xi^{\delta}}\right)\Bigg|_{(0,-1)}^{(0,1)}, \tag{7}$$

where $\varepsilon=\gamma$, $\delta=\beta$ or $\varepsilon=\beta$, $\delta=\gamma$. In order to eliminate spurious pressure modes, the pressure-weighted interpolation method of Reference [9] is employed, but will not be discussed here since this does not affect the discretization.

In order to complete the discretization, the cell face terms in (6) need to be expressed in terms of cell centre values. This is not a trivial matter because, due to the piecewise bilinearity of the co-ordinate mapping, geometric terms such as $\sqrt{g}$ and $\boldsymbol{a}^{(\alpha)}$ are discontinuous at the cell faces. This is discussed in detail in Reference [6]. Three methods will be considered here.

3. THE TWO-POINT METHOD

The TP method has been employed in [1–3], and uses values from the two neighbouring cells. At the cell face $(1,0)$ (cf. Figures 1 and 2), the covariant base vectors $\boldsymbol{a}_{(\alpha)}\equiv\partial x/\partial\xi^{\alpha}$ are evaluated as follows:

$$\boldsymbol{a}_{(1)}=\frac{1}{4}(x_{(3,1)}+x_{(3,-1)}-x_{(-1,1)}-x_{(-1,-1)}),$$
$$\boldsymbol{a}_{(2)}=x_{(1,1)}-x_{(1,-1)}. \tag{8}$$

From this the required quantities are evaluated by well-known identities

$$\sqrt{g}\boldsymbol{a}^{(1)}=(a_{(2)}^{2},\ -a_{(2)}^{1})^{T},\qquad \sqrt{g}\boldsymbol{a}^{(2)}=(-a_{(1)}^{2},\ a_{(1)}^{1})^{T},$$
$$\sqrt{g}=a_{(1)}^{1}a_{(2)}^{2}-a_{(1)}^{2}a_{(2)}^{1},\qquad g^{\alpha\beta}=\boldsymbol{a}^{(\alpha)}\cdot\boldsymbol{a}^{(\beta)}. \tag{9}$$

The cell face quantity $\phi_{(1,0)}$ is approximated as follows:

$$\phi_{(1,0)} = (d_0\phi_{(2,0)} + d_2\phi_{(0,0)})/(d_0 + d_2), \tag{10}$$

where d_n is the distance between $(n, 0)$ and $(1, 0)$. For the case where $(1, 0)$ lies on a straight line between $(0, 0)$ and $(2, 0)$, Equation (10) represents linear interpolation, and the accuracy is satisfactory. However, on strongly distorted grids, $\phi_{(1,0)}$ may be far from collinear with $(0, 0)$ and $(2, 0)$, in which case Equation (10) is likely to be inaccurate.

The derivatives required in (7) are approximated as follows:

$$\left(\frac{\partial\phi}{\partial\xi^1}\right)_{(1,0)} \approx \phi_{(2,0)} - \phi_{(0,0)}, \qquad \left(\frac{\partial\phi}{\partial\xi^2}\right)_{(1,0)} \approx \frac{1}{2}(\phi_{(1,2)} - \phi_{(1,-2)}). \tag{11}$$

Of course, inaccuracy in $\phi_{(1,m)}$ is inherited by this approximation of $\partial\phi/\partial\xi^2$.

For the implementation of velocity boundary conditions, the domain is surrounded by ghost cells in which virtual values are determined by means of the boundary conditions. For the pressure gradient term, this is also done if a boundary condition is given for the pressure. If this is not the case, ghost cells are not used for the pressure, but extrapolation is applied. Assuming that $(1, 0)$ is at the right-hand boundary, one writes

$$p_{(1,0)} = p_{(0,0)} + \frac{d_1}{d_{-2}}(p_{(0,0)} - p_{(-2,0)}). \tag{12}$$

Furthermore, modification is required in the approximation of $(\partial p/\partial\xi^2)_{(1,0)}$ when the $(0, 1)$ cell face is part of the upper boundary. Here one takes

$$\left(\frac{\partial\phi}{\partial\xi^2}\right)_{(1,0)} \approx \frac{3}{2}\phi_{(1,0)} - 2\phi_{(1,-2)} + \frac{1}{2}\phi_{(1,-4)}. \tag{13}$$

If the grid is smooth enough, the TP method gives good results, as shown in Reference [10].

4. THE BILINEAR INTERPOLATION METHOD

With the BI method, cell face values are determined by bilinear interpolation in the physical plane. The point $(1, 0)$ either lies in the quadrilateral spanned by the four cell centres $(0, 0)$, $(2, 0)$, $(2, 2)$ and $(0, 2)$ or in the quadrilateral spanned by $(0, 0)$, $(2, 0)$, $(2, -2)$ and $(0, -2)$. First, it is determined in which of these two quadrilaterals the point $(1, 0)$ is located. Then, $\phi_{(1,0)}$ is expressed in terms of the ϕ values in the vertices of this quadrilateral by means of bilinear interpolation. If it is assumed that $(1, 0)$ is in the first quadrilateral specified above, bilinear interpolation results in an approximation of the following type:

$$\phi_{(1,0)} \approx a_0 + a_1\xi^1 + a_2\xi^2 + a_3\xi^1\xi^2. \tag{14}$$

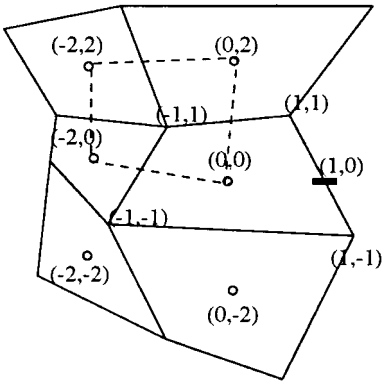

Figure 3. Choice of the quadrilateral close to a boundary.

The coefficients $a_0, \ldots, a_3$ are efficiently computed by means of the Newton–Raphson method. The cell face derivatives $(\partial\phi/\partial\xi^\alpha)_{(1,0)}$ are found by differentiation of (14).

When the cell face is part of a boundary, the point (1, 0) does not lie inside a quadrilateral of the type specified above. Therefore, bilinear extrapolation is used to approximate $\phi_{(1,0)}$. For this, the interior quadrilateral with vertices in cell centres that is nearest to (1, 0) is used, as illustrated in Figure 3.

5. THE PATH–INTEGRAL METHOD

The PI method is described in References [5,6] for a staggered scheme. In Reference [4], one finds the adaptations required for the colocated approach. The point of departure is Equation (3).

The x^γ derivatives of $\boldsymbol{u}$ that appear in the expression for τ_γ^β in (3) are approximated as follows. For a differentiable function ϕ, it is written

$$\phi\big|_{(0,0)}^{(2,0)} = \int_{(0,0)}^{(2,0)} \nabla\phi \cdot \mathrm{d}\boldsymbol{x} \approx (\nabla\phi)_{(1,0)} \cdot \boldsymbol{c}_{(1)}, \quad \boldsymbol{c}_{(1)} \equiv \boldsymbol{x}\big|_{(0,0)}^{(2,0)}. \tag{15}$$

Similarly, for the sum of the two integration paths $(0, -2)$–$(0, 2)$ and $(2, -2)$–$(2, 2)$, you get

$$\phi\big|_{(0,-2)}^{(0,2)} + \phi\big|_{(2,-2)}^{(2,2)} \approx (\nabla\phi)_{(1,0)} \cdot \boldsymbol{c}_{(2)}, \quad \boldsymbol{c}_{(2)} \equiv \boldsymbol{x}\big|_{(0,-2)}^{(0,2)} + \boldsymbol{x}\big|_{(2,-2)}^{(2,2)}. \tag{16}$$

Solving Equations (15) and (16) for $(\nabla\phi)_{(1,0)}$ gives

$$(\nabla\phi)_{(1,0)} \approx \boldsymbol{c}^{(1)}\phi\big|_{(0,0)}^{(2,0)} + \boldsymbol{c}^{(2)}\{\phi\big|_{(0,-2)}^{(0,2)} + \phi\big|_{(2,-2)}^{(2,2)}\}, \tag{17}$$

where

$$\boldsymbol{c}^{(1)} \equiv \frac{1}{C}(c^2_{(2)}, -c^1_{(2)}), \qquad \boldsymbol{c}^{(2)} \equiv \frac{1}{C}(-c^2_{(1)}, c^1_{(1)}), \qquad C \equiv c^1_{(1)}c^2_{(2)} - c^1_{(2)}c^2_{(1)}. \tag{18}$$

Note that this approximation of $\nabla\phi$ does not require smoothness of the grid.

The PI method can also be applied to the pressure term, but was found to be not very accurate for the colocated scheme. A more accurate approximation of the gradient is given by

$$\int_{\Omega_h} \frac{\partial p}{\partial x^\gamma}\,\mathrm{d}\Omega = (\sqrt{g}a^{(1)}_\gamma p)\big|^{(1,0)}_{(-1,0)} + (\sqrt{g}a^{(2)}_\gamma p)\big|^{(0,1)}_{(0,-1)}. \tag{19}$$

The pressure at the face centre is evaluated by the BI method. The remaining terms in (3) are discretized with the BI method.

At the boundaries, the shear stress is approximated in the same way, using ghost cells for the velocity and using the boundary conditions.

A possible source of inaccuracy of the PI method is that, on strongly distorted grids, the evaluation point (1, 0) is far from centred with respect to the cell centres that are used in the integration paths.

6. THE AUXILIARY POINT METHOD

The AUX method is a generalization of a method described in [7] (Section 8.6) to evaluate gradients at cell faces. At both sides of the cell face centre (1, 0) points L and R are chosen at an equal distance from (1, 0) and on the normal through (1, 0), cf. Figure 4. The distance between L and R does not matter much, but should be such that L and R are in the polygon

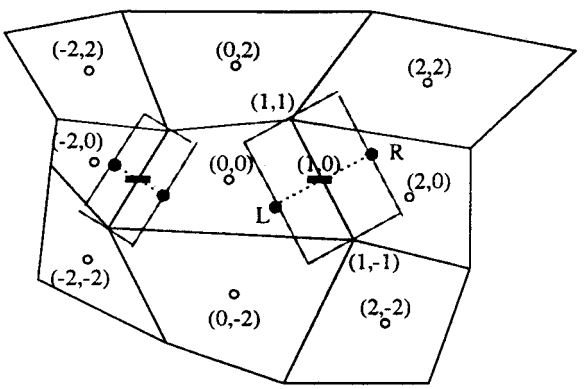

Figure 4. Location of the auxiliary points.

with vertices $(0, 0)$, $(0, \pm 2)$, $(2, 0)$, $(2, \pm 2)$. This can be simply realized in practice, for example, by first choosing $d[(1, 0), L] = d[(1, 0), R] = \frac{1}{5}\min\{d[(1, 0), (0, 0)], d[(2, 0), (1, 0)]\}$, and halving the distance successively until L and R are inside the aforementioned polygon.

By bilinear interpolation, ϕ_L and ϕ_R are expressed in terms of cell centre values. A cell face value $\phi_{(1,0)}$ is obtained by

$$\phi_{(1,0)} = \frac{1}{2}(\phi_L + \phi_R). \tag{20}$$

The pressure term is approximated by (19) and the cell face pressure is given by (20).

In order to approximate derivatives at $(1, 0)$, first $\phi_{(1,\pm 1)}$ is approximated by the BI method between the surrounding cell centres. Normal and tangential derivatives at $(1, 0)$ are easily approximated by means of differences of $\phi_{(1,\pm 1)}$, ϕ_L and ϕ_R. These are easily transformed to approximations of x^α derivatives, or equivalently, the PI method can be used as a convenient way to arrive at the following formulae (cf. Equations (17) and (18)):

$$(\nabla\phi)_{(1,0)} \approx \boldsymbol{c}^{(1)}\phi\big|_L^R + \boldsymbol{c}^{(2)}\phi\big|_{(1,-1)}^{(1,1)},$$

$$\boldsymbol{c}^{(1)} \equiv \frac{1}{C}(c^2_{(2)}, -c^1_{(2)}), \qquad \boldsymbol{c}^{(2)} \equiv \frac{1}{C}(-c^2_{(1)}, c^1_{(1)}), \qquad C \equiv c^1_{(1)}c^2_{(2)} - c^1_{(2)}c^2_{(1)}, \tag{21}$$

$$\boldsymbol{c}_{(1)} \equiv x_R - x_L, \qquad \boldsymbol{c}_{(2)} \equiv \boldsymbol{x}_{(1,1)} - \boldsymbol{x}_{(1,-1)}.$$

The derivatives $\partial u^\beta/\partial x^\gamma$ and $\partial u^\gamma/\partial x^\beta$, which occur in τ^β_γ, are evaluated according to (21).

At the boundaries, the shear stress is approximated in the same way, using auxiliary points. L and R are on both sides of the boundary (cf. Figure 5) and boundary conditions are expressed in terms of function values in L and R. Thus, it is necessary to build the $(2, 0)$ and

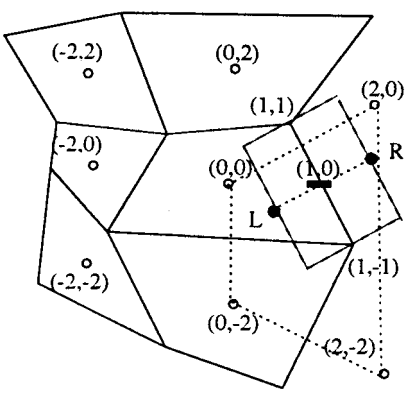

Figure 5. Velocity: L and R at a boundary.

$(2, -2)$ ghost centres to obtain the quadrilateral surrounding L and R. However, it turns out that the $(2, 0)$ and $(2, -2)$ values are coupled and simultaneously unknown. Generalizing this process to all the cells near the boundaries implies that a linear system has to be solved, which is done easily.

If the cell face centre $(1, 0)$ is at a boundary and no pressure boundary condition is given, then $p_{(1,0)}$ is expressed in terms of interior cell centre values by extrapolation, again using auxiliary points. Both auxiliary points are chosen on the interior normal (cf. Figure 6), with the distances satisfying $d[(1, 0), L] = \frac{1}{2}d(L, R)$.

7. BILINEAR INTERPOLATION WITH THE NEWTON–RAPHSON METHOD

The methods described before require frequent use of bilinear interpolation. It pays to do this efficiently. Various methods have been put forward, see e.g. [11,12]. The following method has been found to be efficient. Consider a quadrilateral, the vertices of which are cell centres labelled 1, 2, 3 and 4. Suppose a bilinear function $f(\boldsymbol{x})$, with $f(\boldsymbol{x}_{(m)})$, $m = 1, \ldots, 4$ being given, and suppose that the functional dependence of $f(\boldsymbol{x}_P)$ on $f(\boldsymbol{x}_{(m)})$ is desired. The point P may be inside or outside the quadrilateral. The quadrilateral is mapped onto the unit square by means of a bilinear mapping $\boldsymbol{x} = \boldsymbol{x}(s)$. Obviously, this mapping is given by

$$\boldsymbol{x} = \boldsymbol{x}_{(1)}(1 - s^1)(1 - s^2) + \boldsymbol{x}_{(2)}s^1(1 - s^2) + \boldsymbol{x}_{(3)}s^1s^2 + \boldsymbol{x}_{(4)}(1 - s^1)s^2. \tag{22}$$

The function value $f(\boldsymbol{x}_P)$ depends on $f(\boldsymbol{x}_{(m)})$ as follows:

$$f(\boldsymbol{x}) = f(\boldsymbol{x}_{(1)})(1 - s^1)(1 - s^2) + f(\boldsymbol{x}_{(2)})s^1(1 - s^2) + f(\boldsymbol{x}_{(3)})s^1s^2 + f(\boldsymbol{x}_{(4)})(1 - s^1)s^2. \tag{23}$$

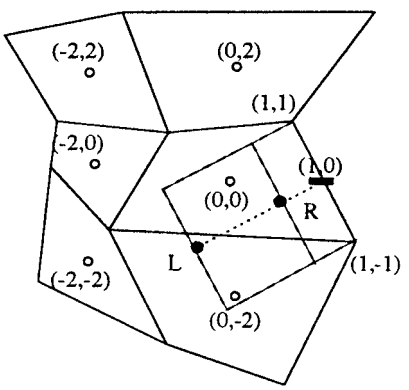

Figure 6. Pressure: L and R at a boundary.

It remains to determine s_P. This is done by substituting $\boldsymbol{x} = \boldsymbol{x}_P$ into Equation (22) and by solving the resulting 2×2 system numerically by the Newton–Raphson iteration.

8. NUMERICAL RESULTS

8.1. Preliminaries

The accuracy of the four schemes presented will be compared by application to a stationary flow with known exact solution and to a flow in an L-shaped channel. The code uses time stepping to steady state and the pressure-weighted interpolation method of Reference [9] to banish spurious pressure modes.

A steady state is assumed to be reached at time $t = (n+1)\Delta t$ if

$$\frac{\|\phi^{n+1} - \phi^n\|}{\|\phi^{n+1}\|} < \varepsilon \frac{1-\lambda}{\lambda}, \tag{24}$$

for all unknowns $\phi = u^1, u^2, p$. Here $\| \ \|$ is the l_2-norm and λ is the rate of convergence to steady state, approximated by

$$\lambda = \|\phi^{n+1} - \phi^n\| / \|\phi^n - \phi^{n-1}\|. \tag{25}$$

The tolerance is $\varepsilon = 10^{-4}$; choosing ε to be smaller was found to make no difference.

To visualize the results post-processing of the numerical solution is required. Most post-processing codes, including the one used by us, require the numerical solution to be given at the vertices of the cells. Hence, for cell centred colocated finite volume schemes, interpolation is necessary. Bilinear interpolation is used for post-processing.

The first test case is a Poiseuille flow. The domain is the rectangle $(0, L) \times (0, 1)$. At $x^1 = 0$, the exact velocity vector is prescribed. At $x^2 = (0, 1)$, the no-slip condition is enforced. At $x^1 = L$, $\partial u^1/\partial x^1 = \partial u^2/\partial x^1 = 0$ is imposed. The exact solution is given by

$$u^1 = 4x^2(1-x^2), \qquad u^2 = 0, \qquad p = 8\nu(L - x^1), \qquad \nu = \mu/\rho.$$

Of course, p is determined only up to a constant. $L = 4$ and $\nu = 0.1$ are chosen, corresponding to $Re = 10$, where Re is the Reynolds number based on the maximum velocity and the height of the channel. The exact pressure drop $\Delta p_e = 3.2$; the exact volume flux $F_e = 2/3$. The numerical volume flux F_h is evaluated at the exit.

The second test case is the flow through an L-shaped channel. The same boundary conditions as for Poiseuille flow are applied. The exact solution is not available.

8.2. Uniform Cartesian grid

To see what accuracy can be obtained on a smooth grid, two uniform Cartesian grids of 15×7 nodes and 27×17 nodes are chosen. On these grids, the four schemes under investigation are identical. On the first grid, the computed pressure drop $\Delta p_h = 3.080$, with a relative error of

3.8% and the computed volume flux $F_h = 0.676$, with a relative error of 1.5%. On the second grid, the computed pressure drop $\Delta p_h = 3.182$, which has a relative error of 0.6%, and the computed volume flux $F_h = 0.660$, with a relative error of 1%. The isobars (not shown) are straight and uniformly spaced, as they should be.

8.3. Moderately distorted grid

Figure 7 shows a moderately distorted grid with 15×7 nodes. Figures 8 and 12 show results obtained with the TP scheme. The isobar pattern is completely unrealistic. The streamlines are quite straight except near the lower and upper walls of the channel. We find $F_h = 0.681$ and $\Delta p_h = 3.321$, which are wrong.

The results obtained with the BI scheme, shown in Figures 9 and 13, are much better. But the streamlines still look like the TP streamlines, and the isobars are not quite straight and uniformly spaced. We find $F_h = 0.685$ and $\Delta p_h = 2.910$.

The results for the PI method are shown in Figures 10 and 14. The isobars are more evenly spaced but no improvement is found for the streamlines. We find $F_h = 0.654$ and $\Delta p_h = 3.098$, which is a significant improvement.

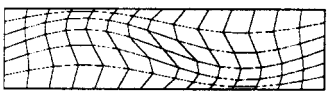

Figure 7. Moderately distorted grid.

Figure 8. Isobars with the TP method.

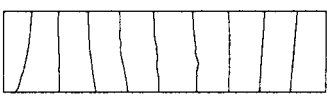

Figure 9. Isobars with the BI method.

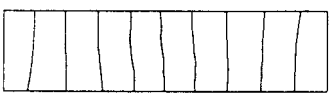

Figure 10. Isobars with the PI method.

Results for the AUX scheme are presented in Figures 11 and 15. The isobar pattern is of the same quality as for PI, but the streamlines are less straight close to the walls. We find $F_h = 0.633$ and $\Delta p_h = 3.059$, which is somewhat less accurate than for PI.

8.4. Highly distorted grid

To further discriminate between the four discretization methods, a more strongly distorted grid is used for the Poiseuille problem. This grid has 27×17 nodes and is shown in Figure 16. For the TP and BI schemes, the solver did not converge. But both the PI and the AUX schemes

Figure 11. Isobars with the AUX method.

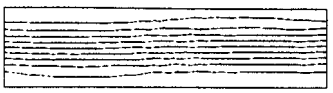

Figure 12. Streamlines with the TP method.

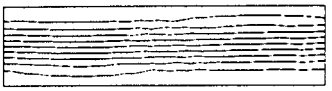

Figure 13. Streamlines with the BI method.

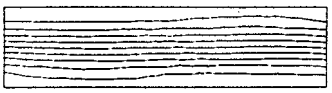

Figure 14. Streamlines with the PI method.

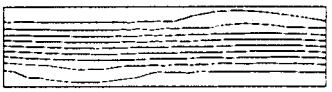

Figure 15. Streamlines with the AUX method.

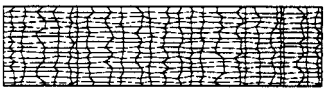

Figure 16. Highly distorted grid.

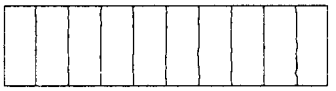

Figure 17. Isobars with the PI method.

Figure 18. Isobars with the AUX method.

give an accurate solution, shown in Figures 17 and 18 for the pressure. In both cases, the isobars are regularly distributed and straight, with results looking slightly better for the AUX near the outlet. The streamlines are not shown because they are straight in both cases. We find $F_h = 0.668$ and $\Delta p_h = 3.210$ for PI and $F_h = 0.660$ and $\Delta p_h = 3.201$ for AUX, which are both close to the values obtained on the uniform 27×17 grid.

8.5. L-shaped channel

Finally, a flow in an L-shaped channel is considered to show the influence of a sharp corner in the geometry. The mesh (cf. Figure 19) is generated by linear interpolation and contains 31×19 cells. The Reynolds number is one. The performance of the PI and the AUX schemes on this mesh are compared. To have some basis of comparison, now that the exact solution in not available, results obtained on the same grid with a finite element method (FEM) using the Q1–P0 element are shown in Figures 20 and 21. The FEM gives $F_h = 0.664$ and $\Delta p_h = 53.499$. The isobars by the AUX method (cf. Figure 23) look more realistic than the ones obtained by the PI method close to the corner (cf. Figure 22), where wiggles appear. For both calculations, the streamlines (not shown) look the same as the FEM ones, including the region near the corner. The PI method gives $F_h = 0.670$ and $\Delta p_h = 54.81$, whereas the AUX method gives $F_h = 0.664$ and $\Delta p_h = 53.891$, which is close to the values obtained by the FEM.

The principles of the PI and the AUX methods carry over to the three-dimensional case. For three-dimensional results with the PI method on staggered grids, see Reference [13].

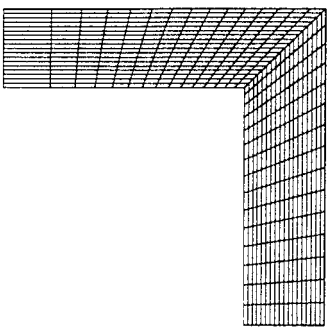

Figure 19. L-shaped grid.

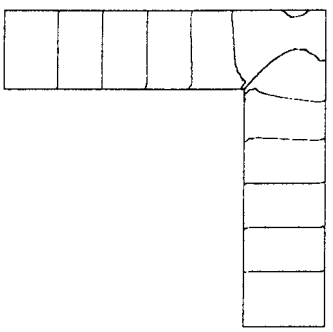

Figure 20. Isobars with the FEM.

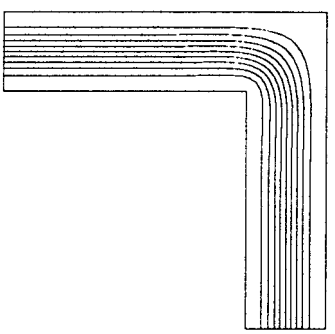

Figure 21. Streamlines with the FEM.

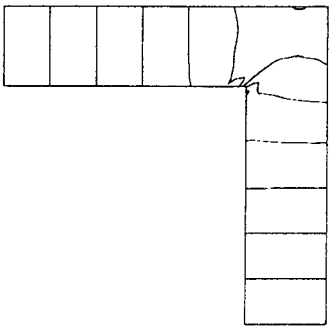

Figure 22. Isobars with the PI method.

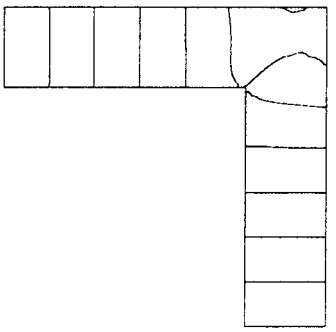

Figure 23. Isobars with the AUX method.

9. CONCLUSIONS

Four colocated schemes for the incompressible Navier–Stokes equations using the pressure-weighted interpolation method of Rhie and Chow [9] have been compared on non-smooth grids. The TP scheme (Section 3, frequently used in the past) is found to be inaccurate on non-smooth grids. The BI scheme (Section 4) is found to be better, but still better are the PI scheme (Section 5) and the AUX scheme (Section 6). The PI and the AUX schemes maintain accuracy on very non-smooth grids.

ACKNOWLEDGMENTS

This study was supported by the Technology Foundation STW.

REFERENCES

1. M. Perić, 'Finite volume method for the prediction of three-dimensional fluid flow in complex ducts', *PhD Thesis*, Imperial College, London, 1985.
2. J. Piquet and P. Queutey, 'Computation of the viscous flow past a prolate spheroid at incidence', in P. Wesseling (ed.), *Proceedings of the Eighth GAMM-Conference on Numerical Methods in Fluid Mechanics*, Notes on Numerical Fluid Mechanics **29**, Braunschweig, Vieweg, 1990, pp. 464–473.
3. W. Rodi, S. Majumdar and B. Schönung, 'Finite volume methods for two-dimensional incompressible flows with complex boundaries', *Comput. Methods Appl. Mech. Eng.*, **75**, 369–392 (1989).
4. C. Moulinec, P. Wesseling, A. Segal and C.G.M. Kassels, 'Colocated discretization of the Navier–Stokes equations on highly non-smooth grids', in C.-H. Bruneau (ed.), *Sixteenth International Conference on Numerical Methods in Fluid Dynamics*, Lecture Notes in Physics **515**, Springer, Berlin, 1998, pp. 85–90.
5. P. van Beek, R.R.P. van Nooyen and P. Wesseling, 'Accurate discretization on non-uniform curvilinear staggered grids', *J. Comput. Phys.*, **117**, 364–367 (1995).
6. P. Wesseling, A. Segal, C.G.M. Kassels, and H. Bijl. Computing flows on general two-dimensional non-smooth staggered grids. *J. Eng. Math.*, 34: 21–44, 1998.
7. J.H. Ferziger and M. Perić, *Computational Methods for Fluid Dynamics*, Springer, Berlin, 1996.
8. R. Aris, *Vectors, Tensors and the Basic Equations of Fluid Mechanics*, Prentice-Hall, Englewood Cliffs, NJ, 1962; reprinted by Dover, New York, 1989.
9. C.M. Rhie and W.L. Chow, 'Numerical study of the turbulent flow past an airfoil with trailing edge separation', *AIAA J.*, **21**, 1525–1532 (1983).
10. I. Demirdžić, Z. Lilek and M. Perić, 'Fluid flow and heat transfer test problems for non-orthogonal grids: bench-mark solutions', *Int. J. Numer. Methods Fluids*, **15**, 329–354 (1992).
11. D. Seldner and T. Westerman, 'Algorithms of interpolation and localization in irregular 2D meshes', *J. Comput. Phys.*, **79**, 1–11 (1988).
12. D.W. Zingg and M. Yarrow, 'A method of smooth bivariate interpolation for data given on a generalized curvilinear grid', *SIAM J. Sci. Stat. Comput.*, **13**, 687–693 (1992).
13. P. Wesseling, A. Segal and C.G.M. Kassels, 'Computing flows on general three-dimensional non-smooth staggered grids', *J. Comput. Phys.*, **149**, 333–362 (1999).

